Groundwater

Case Study/

Risk-Based Decision-Support Groundwater Modeling for the Lower San Antonio River Basin, Texas, USA

by Linzy K. Foster[1,2], Jeremy T. White[3], Andrew T. Leaf[4], Natalie A. Houston[2], and Aarin Teague[5]

Abstract

A numerical surface-water/groundwater model was developed for the lower San Antonio River Basin to evaluate the responses of low base flows and groundwater levels within the basin under conditions of reduced recharge and increased groundwater withdrawals. Batch data assimilation through history matching used a simulation of historical conditions (2006-2013); this process included history-matching to groundwater levels and base-flow estimates at several gages, and was completed in a high-dimensional (highly parameterized) framework. The model was developed in an uncertainty framework such that parameters, observations, and scenarios of interest are envisioned stochastically as distributions of potential values. Results indicate that groundwater contributions to surface water during periods of low flow may be reduced from 6% to 25% with a corresponding 25% reduction in recharge and a 25% increase in groundwater pumping over an 8-year planning period. Furthermore, results indicate groundwater-level reductions in some hydrostratigraphic units are more likely than in other hydrostratigraphic units over an 8-year period under drought conditions with the higher groundwater withdrawal scenario.

Introduction

The lower San Antonio River Basin (herein referred to as "the basin") includes the main stem of the San Antonio River downstream from San Antonio, Texas. The San Antonio River traverses the Texas coastal uplands aquifer system and the coastal lowlands aquifer system as it makes its way toward the Gulf of Mexico where it eventually flows into the Guadalupe River upstream from San Antonio Bay. Stakeholders are interested in understanding the surface-water/groundwater interactions within the basin. There is concern that streamflow and groundwater levels could be adversely affected by both increased groundwater withdrawals and reduced recharge associated with climate variability. Numerical models are useful tools for understanding groundwater-flow systems, estimating specific quantities of interest (such as surface-water/groundwater interactions) under potential forecast scenarios and, most importantly, for guiding water-resource managers in decision making. Furthermore, numerical models in a stochastic framework provide a risk-based assessment of different quantities of interest to guide a more informed decision than a single deterministic estimate would provide. In this analysis, a transient MODFLOW-NWT model (Niswonger et al., 2011) was developed in a stochastic framework to investigate surface-water/groundwater interactions and estimate changes in groundwater levels and low base flows. Batch data assimilation through history matching (e.g., "calibration") (herein referred to as "data assimilation") is

[1]Corresponding author: U.S. Geological Survey, Oklahoma-Texas Water Science Center, 1505 Ferguson Lane, Austin, TX 78754; 512-367-0932; lfoster@usgs.gov

[2]Oklahoma-Texas Water Science Center, U.S. Geological Survey, 1505 Ferguson Lane, Austin, TX, 78754

[3]Intera Inc., Austin, TX

[4]U.S. Geological Survey, Middleton, MI

[5]San Antonio River Authority, San Antonio, TX

Article impact statement: Base flow and groundwater were estimated under uncertainty for the lower San Antonio River Basin in Texas to aid risk-based decision-making.

Received May 2020, accepted April 2021.

doi: 10.1111/gwat.13107

used to condition uncertain model input toward ultimately reducing uncertainty in the simulated spatial and temporal surface-water/groundwater exchange patterns.

Several previous investigations have focused on understanding the hydrology and hydrogeology of the lower San Antonio River Basin. These include gain/loss studies, simulations of streamflow and sediment transport, and simulations of regional groundwater availability. Lizárraga and Wehmeyer (2012) summarized results from a gain/loss survey of the lower San Antonio River from 2006 to 2010 using continuous streamflow records along with discrete observations and found segments of the lower San Antonio River and Cibolo Creek (a main tributary to the lower San Antonio River) where there were surface-water/groundwater interactions. Watershed modeling for the basin focused on simulation of streamflow, evapotranspiration, and groundwater recharge within the basin (Lizárraga and Ockerman 2010) as well as suspended-sediment transport (Banta and Ockerman 2014). Several regional-scale groundwater availability models that encompass the basin were developed for regional water-planning purposes, but these models were not developed with the spatial or temporal resolution to evaluate groundwater/surface interactions in the basin, nor does any particular model encompass the entire basin. These models include the Gulf Coast aquifer (Waterstone 2003; Chowdhury et al. 2004), the Queen City and Sparta aquifers (Kelley et al., 2004), the Carrizo-Wilcox aquifer (Dutton et al. 2003; Kelley et al., 2004), and the Yegua-Jackson aquifer (Deeds et al. 2010). The existing models were used to inform the a priori parameter uncertainty of the model presented herein.

Population for the entire San Antonio River Basin is expected to increase by 73% between 2020 and 2070, with a corresponding increase of 34% in the water demand (South Central Texas Regional Water Planning Group 2015). Furthermore, the basin is located in a large oil and gas production area in Texas referred to as "the Eagle Ford shale play," which reached a peak of 5613 issued drilling permits in 2014 (Railroad Commission of Texas 2019). There is concern that with increased groundwater withdrawals for both municipal use and oil and gas production, the lower San Antonio River and its main tributaries may undergo reductions in groundwater contributions and increased losses into the underlying aquifers. With potential future reductions in recharge attributed to climate variability, streamflow depletion could be further exacerbated. The numerical model we developed was designed to simulate low base flows in the lower San Antonio River and its main tributaries, as well as groundwater levels, for the period of 2006 to 2013. Scenarios of interest were developed to investigate the effects of reduced recharge and increased groundwater withdrawals on streamflow and groundwater levels. The history-matching and scenario simulations were subjected to both linear and nonlinear uncertainty quantification techniques (e.g., Doherty 2015) to account for parameter uncertainty in model-generated outputs.

Description of Study Area

The lower San Antonio River Basin covers about 2150 mi^2 as it extends from south of San Antonio to the Gulf of Mexico. The basin includes about 190 miles of the San Antonio River from the uppermost gage (near Elmendorf) to the confluence of the river with the Guadalupe River, as well as about 75 miles of Cibolo Creek (from the upstream boundary to its confluence with the San Antonio River). The main stems of interest include the lower San Antonio River, Cibolo Creek, and parts of other smaller tributaries (Figure 1). Continuous streamflow records from four main streamgages within the basin (U.S. Geological Survey [USGS] streamgages 08181800 San Antonio River near Elmendorf, Texas, 08183500 San Antonio River near Falls City, Texas, 08186000 Cibolo Creek near Falls City, Texas, and 08188500 San Antonio River at Goliad, Texas) show that the lower San Antonio River is an overall gaining system from the uppermost gage near Elmendorf to the most downstream gage at Goliad. The median of monthly streamflows for 2006 to 2013 are 7.9 m^3/s (or 279 cfs) for Elmendorf, 8.6 m^3/s (or 304 cfs) for San Antonio River near Falls City, 1.3 m^3/s (or 47 cfs) for Cibolo Creek near Falls City, and 11.0 m^3/s (or 387 cfs) for San Antonio River at Goliad (U.S. Geological Survey 2019). The Goliad gage is downstream from the confluence of the Cibolo Creek and the San Antonio River.

The lower San Antonio River traverses several aquifers and confining units that comprise the coastal lowlands aquifer system and the Texas coastal uplands aquifer system (Ryder 1996). The coastal lowlands aquifer system, also known as the Gulf Coast aquifer in Texas, consists of five units: the Chicot aquifer, the Evangeline aquifer, the Burkeville confining unit, the Jasper aquifer, and the "Catahoula" (Ashworth and Hopkins 1995), which is regionally known as the Catahoula confining system (Baker, 1979), but is used in some areas for groundwater (Ashworth and Hopkins 1995) and is therefore conceptualized in this investigation as an aquifer. For this investigation, the Texas coastal uplands aquifer system in this area, which is composed of Eocene deposits of the Claiborne Group and Eocene and Paleocene deposits of the Wilcox Group (Ryder 1996), is divided into eight units: the Yegua-Jackson aquifer, the Cook Mountain confining unit (Deeds et al. 2010), the Sparta aquifer, the Weches confining unit, the Queen City aquifer, the Reklaw confining unit (Kelley et al., 2004), the Carrizo aquifer, and the Wilcox Group, which composes the Wilcox aquifer (Dutton et al. 2003; Mace et al. 2006). The updip extent of the base of the Wilcox aquifer (contact with the underlying Tertiary-age Midway Group) serves as the northwest boundary of the model extent (Figure 2).

The groundwater conditions in Wilson, Karnes, and Goliad Counties are of primary concern in this investigation, as pumping of groundwater in these counties could have the most immediate effect on streamflow. Groundwater use in these counties for 2010 was 7.10 mgd municipal, 14.55 mgd irrigation, 1.01 mgd domestic, and 2.83 mgd

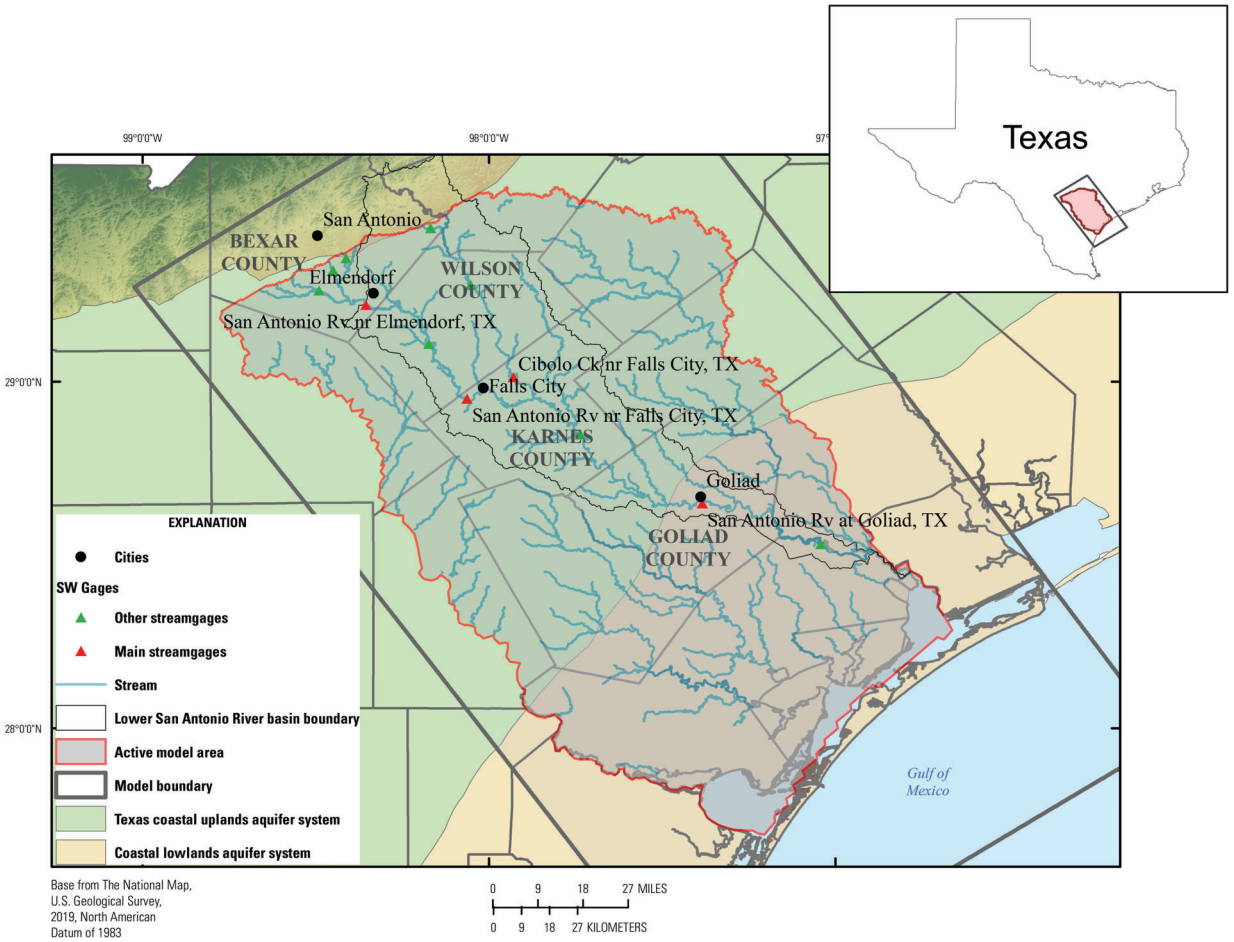

Figure 1. Model extent, lower San Antonio River Basin boundary, surface-water network (blue lines), streamflow gages of primary concern (red triangles), and other streamflow gages (green triangles). Additional model details are provided in the Supporting Information.

stock (Maupin et al. 2014). Water use related to oil and gas production is not reported, but is likely an appreciable component of the groundwater use in Karnes County.

Model Construction and Stochastic Framework

The surface-water/groundwater model of the basin was constructed with MODFLOW-NWT Niswonger et al. (2011) and used the streamflow routing package SFR to simulate surface-water flow and surface-water/groundwater interactions. A simulation period for data assimilation (herein referred to as the "DA simulation") was developed to reproduce historical conditions (2006-2013) to facilitate history matching to system state observations. This time period was chosen because it includes both a wet year (2007) and the driest year on record (2011). Two scenario simulations of interest were also constructed—these scenarios cover the same time period as the DA simulation, but use modified forcings as follows:

- **Scenario 1**: 25% global reduction in recharge and headwater stream inflows +1% global increase in groundwater pumping.
- **Scenario 2**: 25% global reduction in recharge and headwater stream inflows +25% global increase in groundwater pumping.

The "global" reduction in recharge was implemented by scaling the spatially and temporally distributed recharge by the requisite factor. A similar operation was used to adjust simulated groundwater pumping. In this way, the historical spatial and temporal patterns of recharge and groundwater pumping are maintained in the scenarios.

Spatial and Temporal Discretization

Spatial discretization of 400 m by 400 m cells was chosen to best optimize simulation of surface-water/groundwater interactions while maintaining reasonable model run times to enable incorporation of high-dimensional data assimilation (e.g., highly parameterized inversion in Doherty et al. 2010b) and the associated uncertainty analysis. Model layering was based on the conceptual hydrostratigraphy of the system (Figure 3), and the active model depth was set to 5500 feet below land surface because this represents the extent of the majority of groundwater withdrawals.

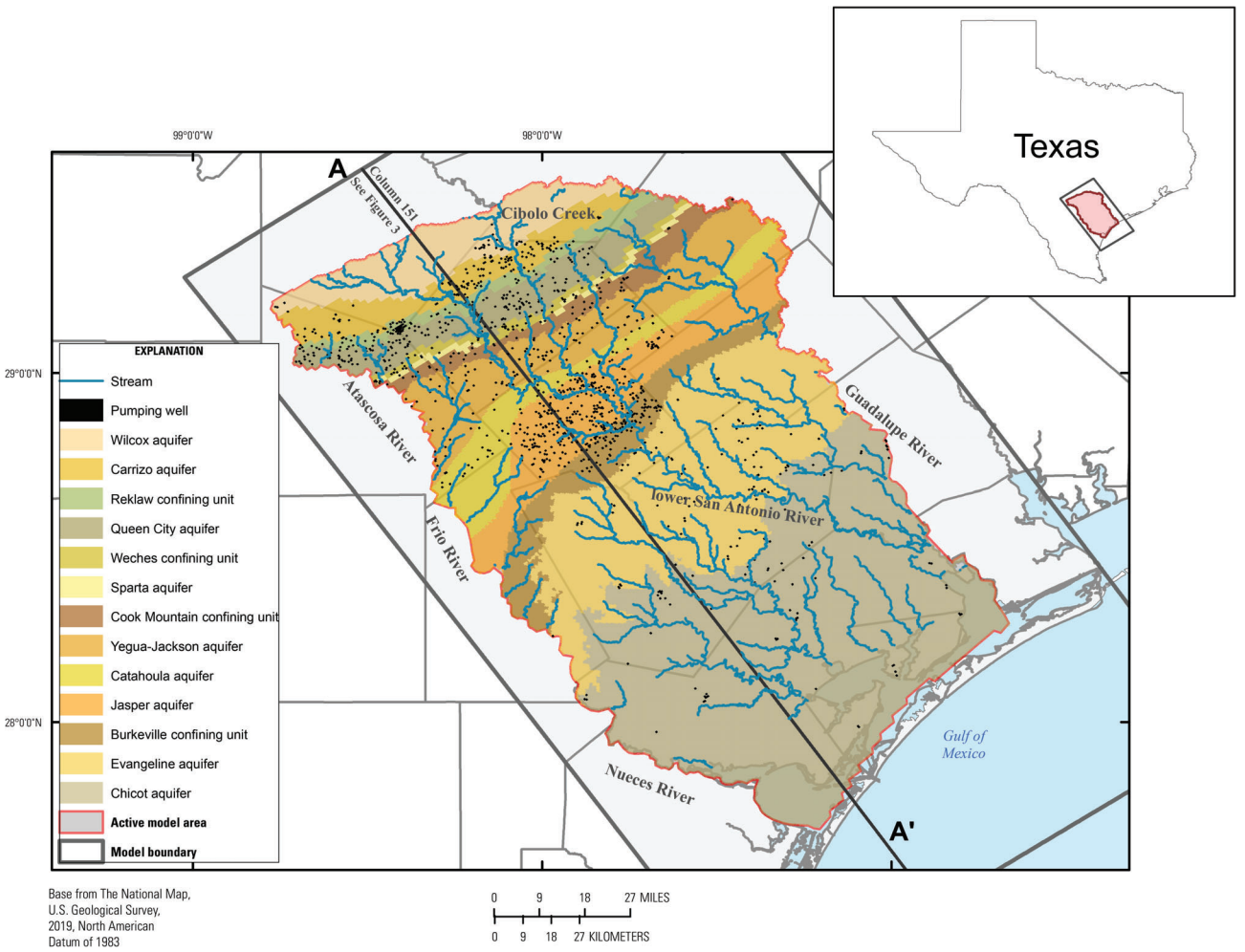

Figure 2. Model extent, surface-water network (blue lines), locations of pumping wells (black solid circles), and the surficial exposure of the aquifers and confining units (corresponding to uppermost model layer) (color map). Also shown is the location of the cross section shown in Figure 3. Additional model details are provided in the Supporting Information.

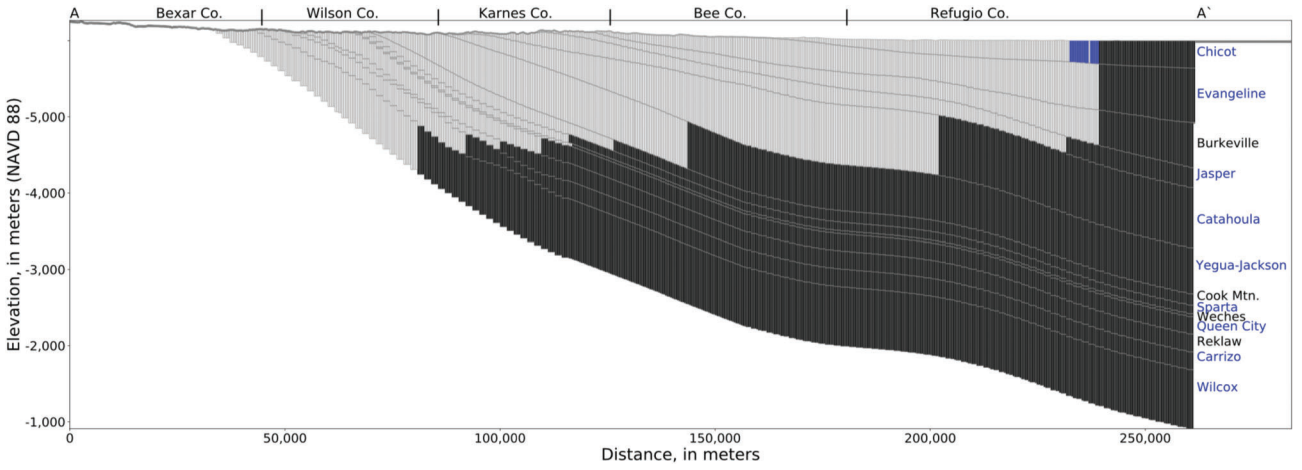

Figure 3. Cross-sectional figure, along column 151, gray cells are active cells, black cells are no-flow cells, blue cells are constant-head cells. Aquifers are labeled in blue and confining units are labeled in black.

MODFLOW-NWT uses a structured grid and does not allow for discontinuous layers. To accommodate the need to continue each of the 13 model layers updip from the outcrop of each unit, layers were carried with a uniform thickness across the study area to the uppermost extent of the model domain. Therefore, layer 1 represents the Chicot aquifer where the Chicot aquifer exists and updip from the surficial extent of the Chicot aquifer, the layer is set to a 10 m thickness representative of the outcrop of each unit it traverses. Layer 2 represents the Evangeline aquifer where it exists and is set to a 1 m thickness updip from the Evangeline aquifer to the northernmost model extent. This layering scheme followed through to the Wilcox aquifer, layer 13, which is the deepest layer and the farthest updip (Figure 2). A similar type of model-layering scheme has been used in other systems with dipping units with distinct outcrop/subcrop areas (Clark and Hart 2009). More information on the active model areas of each layer is provided in the Supporting Information.

The temporal period of the DA simulation encompasses the years 2006 to 2013 (Foster 2020) and includes both a wet year (2007) and the driest year on record in Texas (2011) (Winters 2013). The DA simulation period is also representative of the years during which groundwater withdrawals increased the most for water use related to oil and gas production in Wilson and Karnes Counties. The DA simulation was discretized into monthly stress periods (1) because groundwater pumping estimates, at best, were provided on a monthly scale and (2) in order to capture the seasonality in the model forcings and responses.

Representation of Hydrologic Stresses

The recharge (RCH) package used spatially distributed estimates of recharge based on the national gridded datasets of annual recharge estimates (Reitz et al. 2017). Recharge was applied to the layer representing the surficial extent of the aquifer or confining unit at that location (see the IRCH array in Figure S14). Annual rates ranged from 0.0022 m/year (0.087 in/year) in 2011 to 0.0881 m/year (3.47 in/year) in 2007. Recharge was distributed to monthly values from these annual rates based on the monthly fractions of annual rainfall in the basin.

Surface-water routing of the lower San Antonio River and its main tributaries was simulated using the SFR package (Niswonger and Prudic 2005). Because the model does not include the entire watershed, specified inflows for the San Antonio River and Cibolo Creek were set at the most upstream reach of each stream and were based on base-flow estimates of the nearest upstream gaged reach or a nearby gaged reach (scaled based on the stream reach widths). The SFR was constructed using NHDPlusV2 based on an arbolate sum threshold of 20 km (McKay et al. 2012). This yielded 10,873 reaches within 1099 segments. Specified inflows from wastewater treatment plant effluent data from the U.S. Environmental Protection Agency were included at known discharge points (Amy Settemeyer, Texas Commission on Environmental Quality, 2016, written communication). Surface-water diversions were implemented at known diversion points using reported diversion rates (Cesar Alvarez, Texas Commission on Environmental Quality, 2016, written communication).

Groundwater use included both extraction wells and injection wells. The WEL package was used for pumping/injection simulation with all well-construction data compiled from the Texas Water Development Board (TWDB) Groundwater Database (Texas Water Development Board 2018a), the Evergreen Underground Water Conservation District, the Goliad County Groundwater Conservation District, and the San Antonio Water System (SAWS). Layer assignment for wells was based on screening interval depth where available, then well depth if available, then aquifer code if available. The volumes of groundwater pumped were obtained from TWDB annual water use survey data (Texas Water Development Board 2018b), and were distributed to wells, matching the water-use category of the volumetric rate with the wells with that water use type as their primary use. Monthly rates were used when available, but most data were provided as annual estimates. Annual estimates were distributed evenly to monthly stress periods except in the case of irrigation-water use, which was distributed to monthly rates based on the irrigation factors of Dutton (2004). Injection well rates for the Twin Oaks Aquifer Storage and Recovery facility were provided by SAWS (2015, written communication). Water use related to oil and gas production activity is not collected or estimated by the TWDB. Estimates of produced water reported in FracFocus (Ground Water Protection Council and Interstate Oil and Gas Compact Commission [IOGCC], 2017) for Karnes and Wilson Counties during 2006-2013 were used to estimate water use at wells in Karnes and Wilson Counties in the Eagle Ford Shale region that were provided by the Evergreen Underground Water Conservation District. Annual net pumping rates ranged from 5.7075E7 cubic meters per year (46,272 acre-feet/year) in the wet year of 2007 to 1.20089E8 cubic meters per year (97,358 acre-ft per year) in the extremely dry year of 2011. Locations of pumping wells are shown in Figure 2.

The northwest boundary (most updip extent) was an assumed no-flow boundary. Lateral boundaries were set at the next closest major rivers (Atascosa/Frio/Nueces Rivers to the southwest and the Guadalupe River to the northeast) using general-head boundaries (GHBs) set at an average river stage along each boundary. Average river stage elevations were calculated at streamgages with continuous data during 2006 to 2013 and interpolated between gage locations. The coastal boundary was set as a constant head of 0 m.

Data Assimilation and Uncertainty Analysis Approach

For this study, we use combined regularized least-squares parameter estimation and a First-Order-Second-Moment (FOSM) based Monte Carlo analysis as a stochastic data assimilation process to conduct a quantitative risk-based assessment. Specifically, we used the subspace Gauss-Levenberg-Marquardt (GLM) algorithm

(e.g., Menke 1989; Oliver et al. 2008), augmented with Tikhonov regularization (e.g., Tikhonov and Arsenin 1977; Doherty et al. 2010a, 2010b) to seek the *maximum* a posteriori *(MAP)* parameter estimate—this algorithm is encoded in the open-source tool PESTPP-GLM (White et al. 2020). Using FOSM theory, we estimated the posterior parameter covariance matrix, which, when combined with the *MAP* parameter estimate, forms a multivariate Gaussian posterior parameter distribution. We then drew an ensemble of realizations from this distribution and propagated the ensemble through the scenarios, to yield uncertainty estimates in the important simulated outputs from the scenarios. Below, each component of this process is described. Readers are referred to Doherty (2015), White et al. (2016), and White et al. (2020) and the references cited therein for more background and detailed treatment of the theory underpinning this process.

Parameterization and the Prior

A complex spatial and temporal parameterization scheme was used in an attempt to account for many sources of model-input uncertainty. Parameterization for aquifer properties, using estimates from existing numerical groundwater models that cover parts of the basin, was designed to cover two spatial scales: (1) uniform parameters applied to each layer for each property and (2) spatially distributed multiplier pilot points (Figure S16) applied to each layer for each property. Parameters representing the uniform value of aquifer properties (e.g., "constant") of horizontal hydraulic conductivity, vertical hydraulic conductivity, specific yield, and specific storage were used for each of the 13 aquifers and confining units. Spatial parameterization using multiplier pilot points, spaced 4 km apart complements the uniform-by-layer values to allow flexibility to capture heterogeneity in each unit for the aquifer properties. Multiplier pilot points were also used for spatial adjustment of recharge. Parameters were also specified for the general-head boundary hydraulic heads and conductance values. Streambed conductance in the SFR package was parameterized on the basis of reaches within the same unit being grouped together (i.e., reaches in the lower San Antonio River traversing the Chicot aquifer were in one parameter group, reaches traversing the surficial exposure of the Evangeline aquifer were in another parameter group, etc.). The SFR conductance grouping is based on the assumption that streambed conductances are correlated across the underlying units but can vary independently of the properties of the underlying units.

To account for potential uncertainty in groundwater recharge and groundwater pumping rates, temporal multiplier parameters were applied to recharge and groundwater pumping. The use of temporal multiplier parameters provided flexibility and helped compensate for any biases in these rates. Annual multiplier parameters were applied to the groundwater recharge rates and multiplier parameters at the stress-period scale (monthly) were applied to the groundwater pumping rates.

The a priori bounds of parameter understanding (see Table 1 and Anderson et al. 2015 for discussion of the prior), as well as the prior expected values, are based on conservative literature values and previous models in the area (Dutton et al. 2003; Waterstone 2003; Chowdhury et al. 2004; Kelley et al., 2004; Deeds et al. 2010). Bounds on spatial and temporal parameters were expanded beyond reported values to allow for additional potential flexibility in the data assimilation process.

Observations and the Likelihood Function

The intended use of the model presented herein is to estimate low base flows and groundwater levels; therefore, these types of observations were used in the data assimilation process. A total of 1083 surface-water discharge observations at 12 sites and 3050 groundwater-level observations at 317 sites were used toward the goal of reducing uncertainty in parameters, and, ultimately, forecasts of low base flows and groundwater levels.

Table 1
A Priori Parameter Summary

Type	Count	Initial Value	Upper Bound	Lower Bound	St. Deviation
Horizontal hydraulic conductivity (C)	13	[−1.5, 0.57]	[1, 3.4]	[−6, −2]	[1, 2]
Specific storage (C)	13	[−5.7, −2.6]	−2.5	−7	1.1
Specific yield (C)	13	[−3.1, −0.42]	[−0.78, −0.42]	[−4, −2.3]	[0.38, 0.90]
Vertical hydraulic conductivity (C)	13	[−4.1, −0.86]	[−1.5, 2.7]	[−8.5, −4.3]	[1.1, 1.8]
GHB conductance	129	[−0.097, 0.04]	2	−2	1
GHB head	226	[−1.1, 0.14]	0.14	−1.1	0.32
Horizontal hydraulic cond. (PP)	631	[−1.1, 2.1]	3	−3	1.5
Recharge	223	[−1.1, 0.14]	0.14	−1.1	0.32
Specific storage (PP)	631	[−0.25, 0.41]	1	−2	0.75
Stream bed cond. (units of m/d)	14	[−0.59, 0.27]	1.5	−4	1.4
Specific yield (PP)	631	[−2, 0.041]	0.041	−2	0.51
Vertical hydraulic conductivity (PP)	423	[−0.63, 0.48]	2	−3	1.3
Well pumping rate	97	[−1.3, 0.30]	0.30	−1.3	0.40

"C" refers to spatially or temporally constant parameters (applied uniformly) and "PP" refers to spatially distributed pilot-point parameters. Square brackets show range of values. All values are log transformed.

Given that the DA simulation uses monthly stress periods and lacks land-surface processes, it would be inappropriate to attempt to reproduce surface-water discharge observations, which represent both low-flow and flooding conditions. Instead, estimating low base flows was the focus of the DA simulation. Surface-water discharge time series were passed through a base-flow index (BFI) filter (Wahl and Wahl 1995) using the USGS Groundwater Toolbox (Barlow et al. 2015) with the number of days (N) equal to 5 days and turning point test factor (f) equal to 0.9. Additionally, to mitigate the ill-effects of structural error in the model (e.g., White et al. 2014), we also included first-order temporal variation observations, constructed by subtracting each observation in a given groundwater level times series (or base-flow time series) from the preceding observation (temporally). This type of processed observation data can steer the data assimilation algorithm to match changes in observations as well as the observations themselves. We acknowledge that several forms of processed surface-water flow observations could be used to provide historical surface-water/groundwater exchange information in the data assimilation process. The approach we selected is well-aligned with the overall goals of the modeling analysis (prediction of low-flow response at surface-water observation locations to changes in forcing), which helps to place the scenario-sensitive parameters (and parameter combinations) more into the solution space of the data assimilation process (e.g., Doherty and Welter 2010; Doherty and Moore 2019).

We used a subjective likelihood function to focus the data assimilation process toward reproducing the components of observed states that most resemble the outputs of management interest (e.g., Doherty and Welter 2010). Drier hydrologic condition replication is of primary concern in this investigation; therefore, it was of primary importance that the data assimilation process focus on replicating low base flows, even if this is at the expense of replicating high-flow conditions. As a result, the weighting scheme used in the data assimilation algorithm was designed to focus more heavily on streamflow during drier conditions at the four main gages. Processed base-flow observations were split into wet (January 2006 to May 2008) and dry (June 2008 to December 2013) conditions. The observed and processed observations for the four main gages of interest (Figure 1) were weighted to contribute more to the composite likelihood function than the processed base-flow observations at other gages. The observation types used for data assimilation contributed to the likelihood function in the following percentages:

- absolute groundwater levels 20% (count = 7711).
- first-order groundwater level temporal differences 20% (count = 7394).
- dry-season base flow and base-flow temporal differences at four gages 40% (count = 536).
- wet-season base flow and base-flow temporal differences at four gages 16% (count = 228).
- base flow and base-flow differences at remaining gage locations 4% (count = 1390).

This weighting scheme was selected such that the primary focus of the analysis is well represented (e.g., dry-season low base flows and dry-season low base-flow rates of change). Some additional focus was also placed on representing groundwater levels and rates of groundwater change, because the ability to robustly simulate the relation between groundwater system changes in forcing and the resulting changes in surface-water/groundwater exchange must propagate through the groundwater system.

Uncertainty Analyses

The data assimilation process provides a necessary parameter set (MAP) representative of the posterior central tendency of the DA simulation for the time period of 2006 to 2013 (e.g., Oliver et al. 2008). This process allows the model to replicate conditions during the 2006 to 2013 time period, but is not sufficient in itself to provide a robust analysis of the model's ability to predict (i.e., estimate quantities of management interest within the scenario simulations). Parameter and scenario output uncertainty analyses (UA) were undertaken so that the results of our modeling analysis provide stakeholders and decision makers with an understanding of the reliability of the important simulated outcomes. We used FOSM uncertainty analyses to estimate the posterior parameter covariance matrix (e.g., Menke 1989; Doherty 2015; White et al. 2016). This covariance matrix was used to generate a pre-conditioned posterior parameter ensemble to run through the DA simulation and the two scenarios of interest.

The FOSM-based posterior parameter covariance matrix is calculated as:

$$\overline{\boldsymbol{\Sigma}}_{\boldsymbol{\theta}} = \boldsymbol{\Sigma}_{\boldsymbol{\theta}} - \boldsymbol{\Sigma}_{\boldsymbol{\theta}}\mathbf{J}^T[\mathbf{J}\boldsymbol{\Sigma}_{\boldsymbol{\theta}}\mathbf{J}^T + \boldsymbol{\Sigma}_{\boldsymbol{\varepsilon}}]^{-1}\mathbf{J}\boldsymbol{\Sigma}_{\boldsymbol{\theta}} \quad (1)$$

where $\boldsymbol{\Sigma}_{\boldsymbol{\theta}}$ is the prior parameter covariance matrix, $\boldsymbol{\Sigma}_{\boldsymbol{\varepsilon}}$ is the epistemic observation noise covariance matrix, and $\mathbf{J}$ is the Jacobian matrix of partial first derivatives of observations with respect to parameters. We used the final Jacobian matrix from application of PESTPP-GLM as the $\mathbf{J}$ in Equation 1. In an attempt to account for irreducible residuals, we applied residual-based reweighting to form $\boldsymbol{\Sigma}_{\boldsymbol{\varepsilon}}$ using the final residuals from the data assimilation process so that the final $\mathcal{L}_2$ norm (also known as the Euclidean norm) of the residuals was equal to the number of non-zero weighed observations (Bonesky 2008; White et al. 2020).

A 100-member parameter ensemble was drawn from the posterior multi-variate Gaussian distribution $\mathcal{N}(\overline{\boldsymbol{\mu}}_{\boldsymbol{\theta}}, \overline{\boldsymbol{\Sigma}}_{\boldsymbol{\theta}})$, where $\overline{\boldsymbol{\mu}}_{\boldsymbol{\theta}}$ are the final parameter values from the PESTPP-GLM (White et al., 2020) analysis (the MAP estimate). The realized values for temporal forcing parameters (those adjusting well pumpage and recharge in the DA and scenario simulations) were derived solely from the prior parameter distribution, instead of the posterior, as these parameters are not conditioned on observation data from the past and therefore, exhibit a higher degree of uncertainty than those conditioned in the

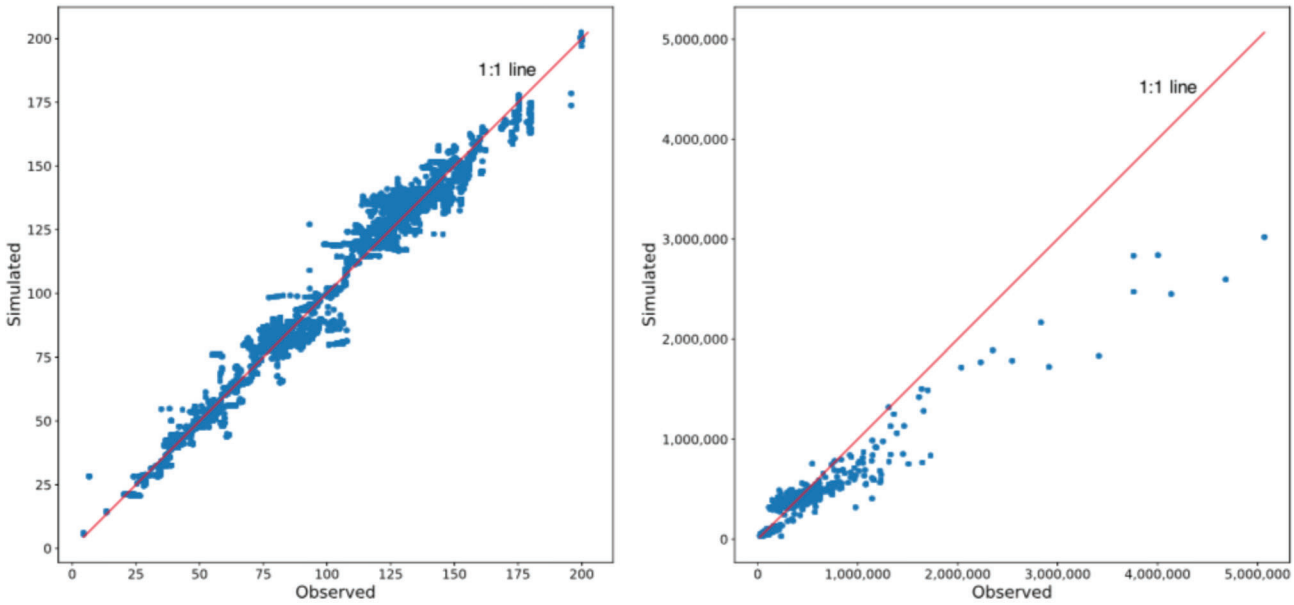

(a) 1:1 plot for hydraulic heads

(b) 1:1 plot for base flows at the four main gages on the San Antonio River (fig. 1)

Figure 4. DA simulation 1:1 plots. Generally, the fit to groundwater levels (hydraulic heads) and low base-flow conditions is unbiased and clustered around the 1:1 line. Some bias is present in the higher base-flow values.

data assimilation process. These prior-based values combined with the maintained spatial and temporal patterns for recharge and groundwater pumping in the scenario simulations provides a robust and conservative representation of the expected uncertainty in model forcing inputs.

The posterior parameter ensemble members were then evaluated with the DA simulation and the two scenario simulations. The resulting output ensembles were used to estimate the posterior uncertainty in the low base flows and groundwater levels under historical forcing conditions (represented by the DA simulation) as well as under hypothetical drought conditions (with increased groundwater withdrawals) represented by the scenarios. Herein, we refer to the output ensemble from the unaltered DA simulation as the *base* ensemble; the output ensembles from Scenario 1 and Scenario 2 are compared to the *base* ensemble for comparative context.

Results of the Data Assimilation and Uncertainty Analysis

Data assimilation with PESTPP-GLM yielded the *MAP* parameter set that replicated historical observations of groundwater levels and low base-flow estimates at streamgages, especially for drier conditions (Figure 4), which is well aligned with the predictive goals of the modeling analysis. Time series of the simulated base flow at the main gages are included in Supporting Information, along with the *MAP* parameter values and posterior standard deviations for each parameter group.

Some limitations exists in the ability to simulate higher base-flow values. This is not unexpected because an imperfect model cannot be expected to simulate all facets of historical system behavior, and, because of this, we purposefully focused the data assimilation process on replicating dry-season base-flow values, meaning the data assimilation process was given leeway to sacrifice the ability to reproduce higher base-flow values if it led to a better reproduction of lower base-flow values. Additionally, higher base-flow values are associated with periods of increased precipitation, which results in land-surface processes becoming increasingly important to simulate surface-water flow conditions—processes which are not included in the model and that are not represented by the temporal discretization that was selected.

The results of the 100-member *base* ensemble show variability in model-generated results owing to uncertainty in the model parameters. The gray-shaded areas represent the range of results (Figure 5). Higher variances were observed during times of higher surface-water flows. Simulated base-flow results at the Elmendorf gage (Figure 5a) show little variability compared to results at farther downstream gages at Goliad (Figure 5d). Variability in the simulated Cibolo Creek base flow at the Cibolo gage, which is upstream from the confluence of Cibolo Creek with the San Antonio River, contributes to the variability in simulated base flow at the Goliad gage downstream.

Simulated Response to Drought and Increased Groundwater Withdrawals

The simulated output ensembles from the DA and scenario simulations were used to stochastically estimate the effects of drought and increased groundwater withdrawals on the surface-water/groundwater exchange and on groundwater levels within the basin. Herein, we define Q95 as the simulated base flow that is equaled

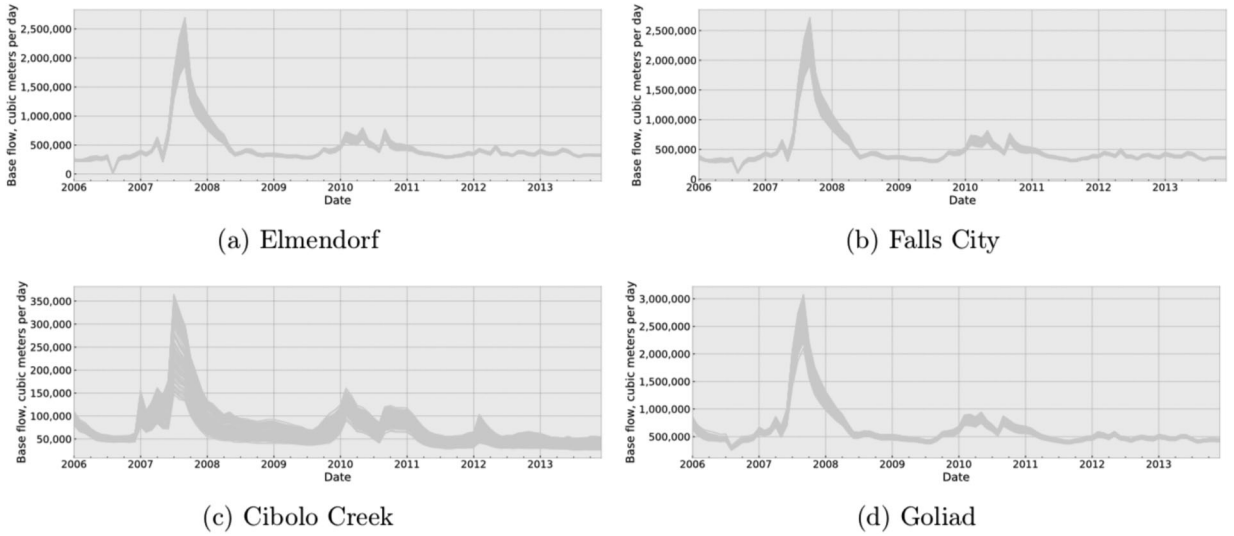

Figure 5. Simulated base flows from the *base* ensemble (also known as the posterior DA simulation ensemble). Wider widths in the ensemble of hydrographs for a given streamgage indicate more variability in simulated base flows compared to narrower widths in the ensemble of hydrographs.

or exceeded 95% of the time. The changes in surface-water/groundwater exchange were evaluated by comparing the Q95 distributions of the *base* ensemble and scenario ensemble results and by comparing the differences in Q95. The Q95 statistic is considered sufficiently representative of low base flows (in this instance). The changes in groundwater levels were evaluated by mapping the changes in the surficial layer and comparing results within different zones where each zone corresponds to the surficial exposure of an aquifer or confining unit.

Generally, the ensemble of simulated base-flow time series (Figure 5) show the smallest amount of uncertainty for the Elmendorf gage which is expected given that this is the farthest upstream gage in the surface-water system and reflects effects from fewer (uncertain) parameters. Time-series differences (e.g., changes) (Figures S22 to S29) were also calculated because differences tend to cancel out model error propagated through to results (White et al. 2014; Knowling et al. 2019). Differences are calculated by subtracting scenario ensemble members from the corresponding members of the *base* ensemble. Ensembles of differences show greater variation during times of higher surface-water flow and less variation in lower-flow conditions; ensembles of differences show the highest degree of uncertainty at Cibolo Creek and Goliad gages.

Changes in Low Base Flows

The potential for changes in low base flows at the four gaging locations of interest was summarized with the Q95 statistic and changes in the Q95 statistic between the *base* scenario and the two drought/pumping scenarios. The Q95 statistic in this investigation is representative of the lowest 5% of base flow for the 8-year transient model period of 2006 to 2013. Both absolute and difference Q95 statistics were computed to gain understanding of low base flows and how these low-flow statistics might change owing to changes in hydrologic stresses. Each ensemble member has a Q95 value for the 8-year period, so the 100 ensemble members produced 100 Q95 statistics for each of the *base* and scenario runs. The difference statistics express the expected statistical change in low base flow resulting from hypothetical drought combined with increased groundwater withdrawals. The difference Q95 statistics were calculated by subtracting the scenario ensemble from the *base* ensemble and calculating a Q95 statistic of the difference. Absolute Q95 values and difference Q95 values were visualized using histograms and were evaluated based on their median and maximum values.

In general, absolute Q95 distributions indicate subtle shifts left from the *base* to scenario 1 and scenario 2 which are indicative of decreases of the Q95 statistics, corresponding to lower-flow conditions in the surface-water network from drought and increases in pumping (Figure 6 [first three columns]). Subtleties in the shifts in the distributions in the first three columns are more apparent in the difference Q95 statistic distributions (the two rightmost columns of Figure 6). Q95 results for scenario 1 and 2 were fairly similar to the Q95 statistic from the *base* ensemble for the Elmendorf gage (Figure 6)—this is not unexpected, given the upstream location of this gage within the model domain and the little variation seen at this gage in the *base* ensemble results. The upstream location of the Elmendorf gage means fewer uncertain parameters contribute to uncertainty of low base flow here as compared to downstream gages. The median Q95 reductions for scenario 1 and 2 were 113 and 1160 m^3/d, respectively, which correspond to a 0.04% and 0.44% decrease in the median Q95 from the *base* ensemble (Table 2). At worst case, low base flow at Elmendorf might be reduced by 0.62% for scenario 1 and 1.33% for scenario 2. This was an order of magnitude (or more) smaller than the simulated changes in low

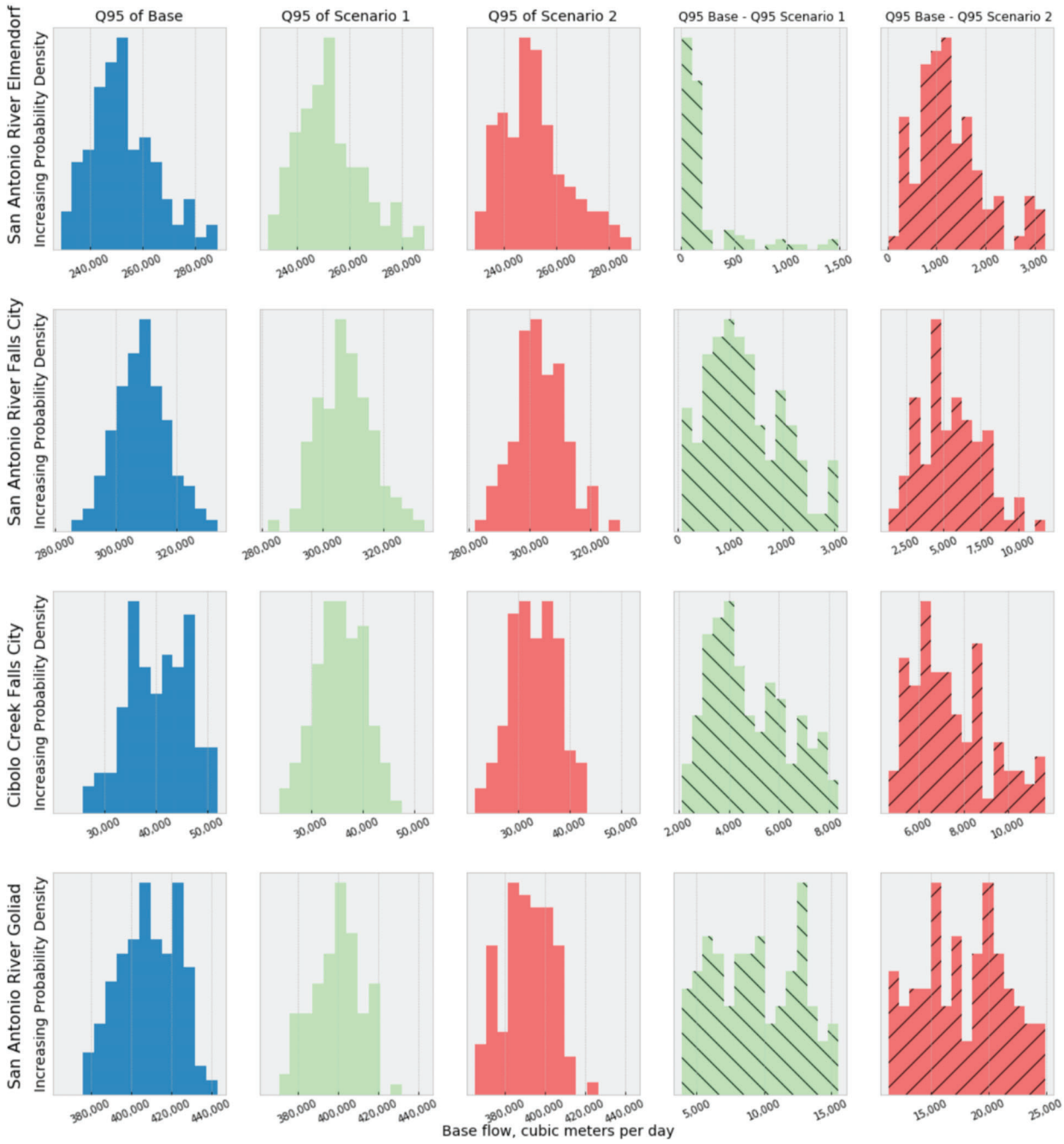

Figure 6. Q95 distributions and difference of Q95 distributions for *base*, scenario 1, and scenario 2 ensembles.

base flows at downstream gages. Low base-flow estimates at the Cibolo Creek gage had the largest percentage reductions for the two scenarios. Scenario 2 may result in as large as a 25.03% reduction in low base flow at this gage (Table 2). Although this was the largest percentage reduction, the base-flow Q95 changes are smaller than those seen at the Goliad gage because base flows in general are higher at the Goliad gage. Simulated low base flow at the Goliad gage exhibited reductions of as much as 3.62% for scenario 1 and 5.89% for scenario 2.

The Q95 distributions, just like the ensemble results they are based on, exhibit varying degrees of uncertainty (Figure 6). In general, the uncertainty of results from scenario 2 is larger than the uncertainty of results from scenario 1. In addition, uncertainty in Q95 results increased in the downstream direction (i.e., from Elmendorf to Goliad), which is expected as downstream sections of the drainage basin are affected by uncertainty throughout larger portions of the model domain, and therefore by more parameters.

Changes in Groundwater Levels

Changes in groundwater levels can affect streamflow, and groundwater levels can decrease when there are reductions in recharge and increases in groundwater withdrawals. Decreases in groundwater levels (particularly

Table 2
Q95 Difference Statistics for 2 Scenarios

Gage	Scenario	Median Q95 Change (m^3/d)	Median Q95% Change	Max Q95% Change
Elmendorf	1	113	0.04	0.62
Elmendorf	2	1160	0.44	1.33
Falls City	1	1148	0.37	1.02
Falls City	2	5319	1.71	3.63
Cibolo Ck	1	4547	11.18	17.80
Cibolo Ck	2	7091	17.84	25.03
Goliad	1	9250	2.29	3.62
Goliad	2	17,662	4.43	5.89

in the shallow groundwater system) are of interest to stakeholders and decision makers because many industrial and domestic users rely on shallow groundwater in the basin. Therefore, an improved understanding of potential changes in groundwater levels could aid in groundwater management and water-use planning. Groundwater-level declines were quantified and visualized through mapping of declines in the surficial layer and through time series of groundwater levels at monitoring wells (wells used for history-matching) (see Figures S30 to S346).

Groundwater-level observations were recorded at the end of the *base* ensemble and scenario ensemble time periods for each active cell of the surficial layer for each ensemble member. Groundwater levels for the scenario ensembles were subtracted from those of the *base* ensemble to quantify the difference of groundwater levels for each scenario. These are referred to as the ensembles of differences. The median and standard deviation of the groundwater-level difference for each cell in the model was calculated for each ensemble of difference (Figure 7). In general, small groundwater-level differences (less than 1 m) are expected for most of the study area for both scenarios, but median reductions in excess of 5 and 12 m are seen in certain areas for scenario 1 and scenario 2, respectively. Areas of higher variance tend to correspond with areas of larger groundwater-level reductions and areas of lower variance tend to be in areas of smaller reductions.

Higher variabilities and larger groundwater-level reductions are seen in some areas of the basin when compared to other areas of the basin. To focus on the individual aquifers that are more prone to groundwater-level reductions, the surficial exposure of the aquifers (Figure 2) were used to analyze the results shown in Figure 7. Median and maximum groundwater-level reductions were calculated for each aquifer for the shallow groundwater system (layer 1) and plotted on a log-scale (Figures 8 and 9). A change of 1 on a log scale equates to 10 m of change, while a change of −5 is a very small change of 0.00001 m. Median groundwater-level differences for scenario 1 are up to 4 m for most water-bearing units, with the largest differences of more than 5 m corresponding to groundwater levels in the Wilcox aquifer (Figure 8a). For scenario 2, most units experienced substantial reductions in groundwater levels when compared to scenario 1, except for the Chicot and the Evangeline aquifers which remained similar to scenario 1 (Figure 8). For the Jasper, Catahoula, and Yegua-Jackson aquifers, the upper bound of the median of the groundwater-level differences increased, whereas increases for the Sparta, Queen City, Carrizo, and Wilcox aquifers were seen in the distributions themselves, not just limited to the upper bounds. In general, the majority of median groundwater-level differences are 1 m or less. Maximum groundwater-level differences for each aquifer for the surficial layer indicate the Carrizo aquifer is expected to have the smallest groundwater-level reduction when compared to other aquifers (Figure 9). The largest potential maximum reductions in groundwater levels are forecast for the Wilcox, Sparta, Yegua-Jackson, Catahoula, and Evangeline aquifers. Large groundwater-level reductions are outliers on the violin plots, and therefore, tend to be derived from localized changes around individual wells. The majority of maximum groundwater-level declines, indicative of the unit as a whole, are 5 m or less. In addition, time series of groundwater levels at monitoring wells (Figure S30 to S346) used for history matching show site-specific effects of the scenarios throughout the study area and at different depths.

Discussion and Conclusion

The combined DA-uncertainty analysis process provides a useful tool for the lower San Antonio River Basin to make estimates of both surface-water/groundwater exchange and groundwater levels within a stochastic framework. We have shown that a fair amount of uncertainty exists in simulated outcomes of management interest, namely changes in low base flow and shallow groundwater levels within the basin during dry conditions. We have also shown that these critical uncertainties vary both spatially and temporally. By placing the important simulated outcomes into a stochastic setting, we can see how the scenarios change not only the central tendency of the important simulated outcomes, but also give estimates of the more extreme outcomes, such as the maximum groundwater-level difference and the maximum Q95 change. These extreme outcomes can be valuable in the decision making setting as they provide important end-member outcomes. Difference outcomes were focused on during this investigation to minimize effects of model error on the important simulation outcomes.

Results of this investigation are conditional upon the model itself (and the assumptions therein), the data used for the data assimilation process, the hydrologic time period simulated, and the prior parameter uncertainty. The ensembles were drawn from the posterior, which was created using FOSM-approximated posterior parameter distribution. Therefore, the analysis is also somewhat dependent upon the linearity assumption of FOSM (i.e., uncertain parameters linearly related to the historical

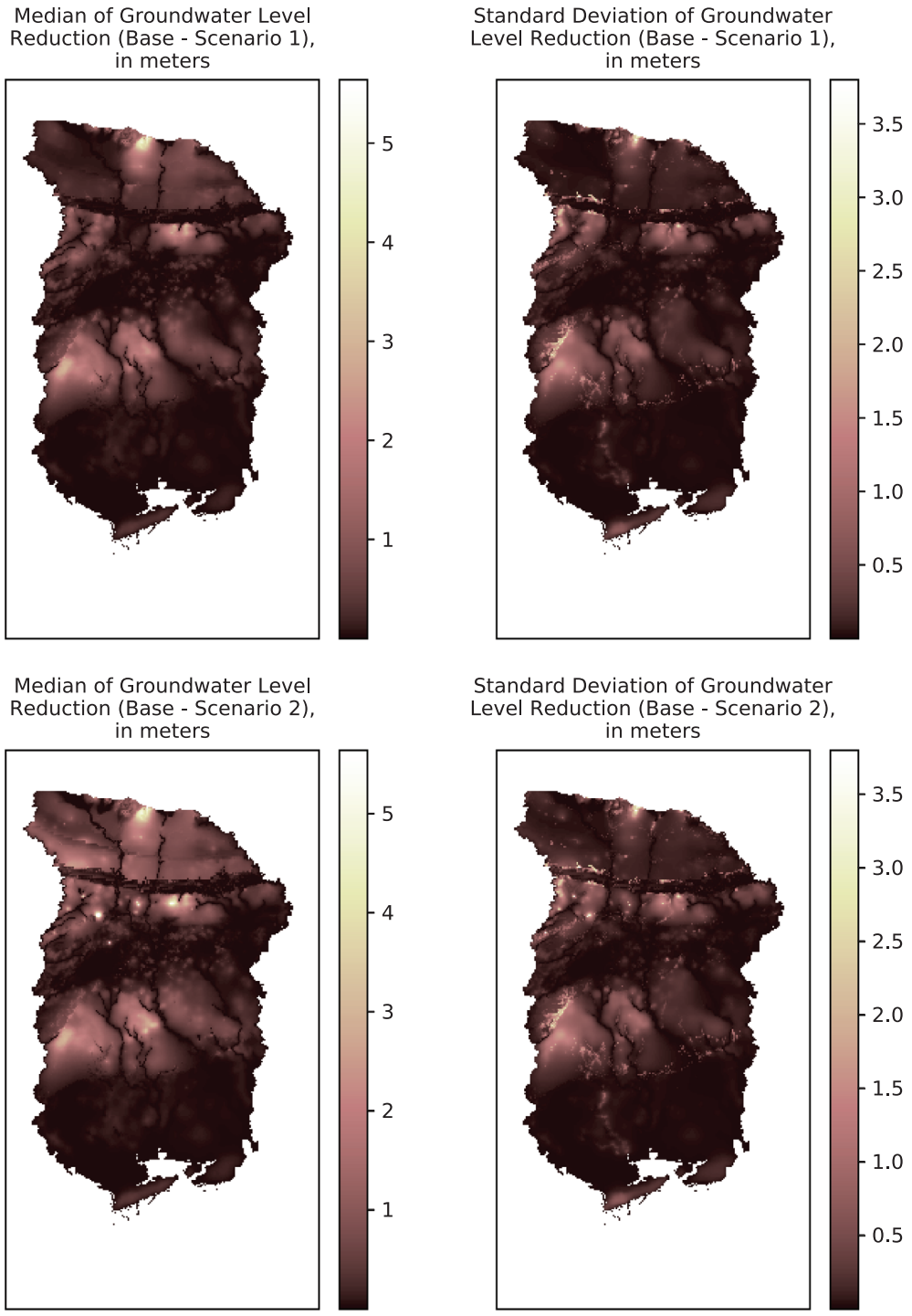

Figure 7. Groundwater-level reductions in the surficial layer. The model grid is rotated 35° in the clockwise direction about the upper left hand corner of the grid at Universal Transverse Mercator zone 14 N easting 497,592 m and northing 3,238,294 m.

estimates of base flow and historical observations of groundwater levels). Furthermore, some hydrologic components (such as surface-water diversions and wastewater treatment plant effluents into the surface-water) were assumed to remain the same during scenario conditions and therefore, were not varied as a part of the scenario uncertainty analysis.

Difference time series indicate a low-frequency temporal trend in the differences between scenario ensemble results and the *base* ensemble (Figures S22 to S29). There is a temporal component to surface-water/groundwater exchange and longer planning cycles may predict larger effects on the surface-water system owing to reduced recharge and increased groundwater pumping. Conditions at the end of the predictive period returning to "normal" would not cause base flows and groundwater levels to immediately rebound, as delays in groundwater responses can continue to cause effects on

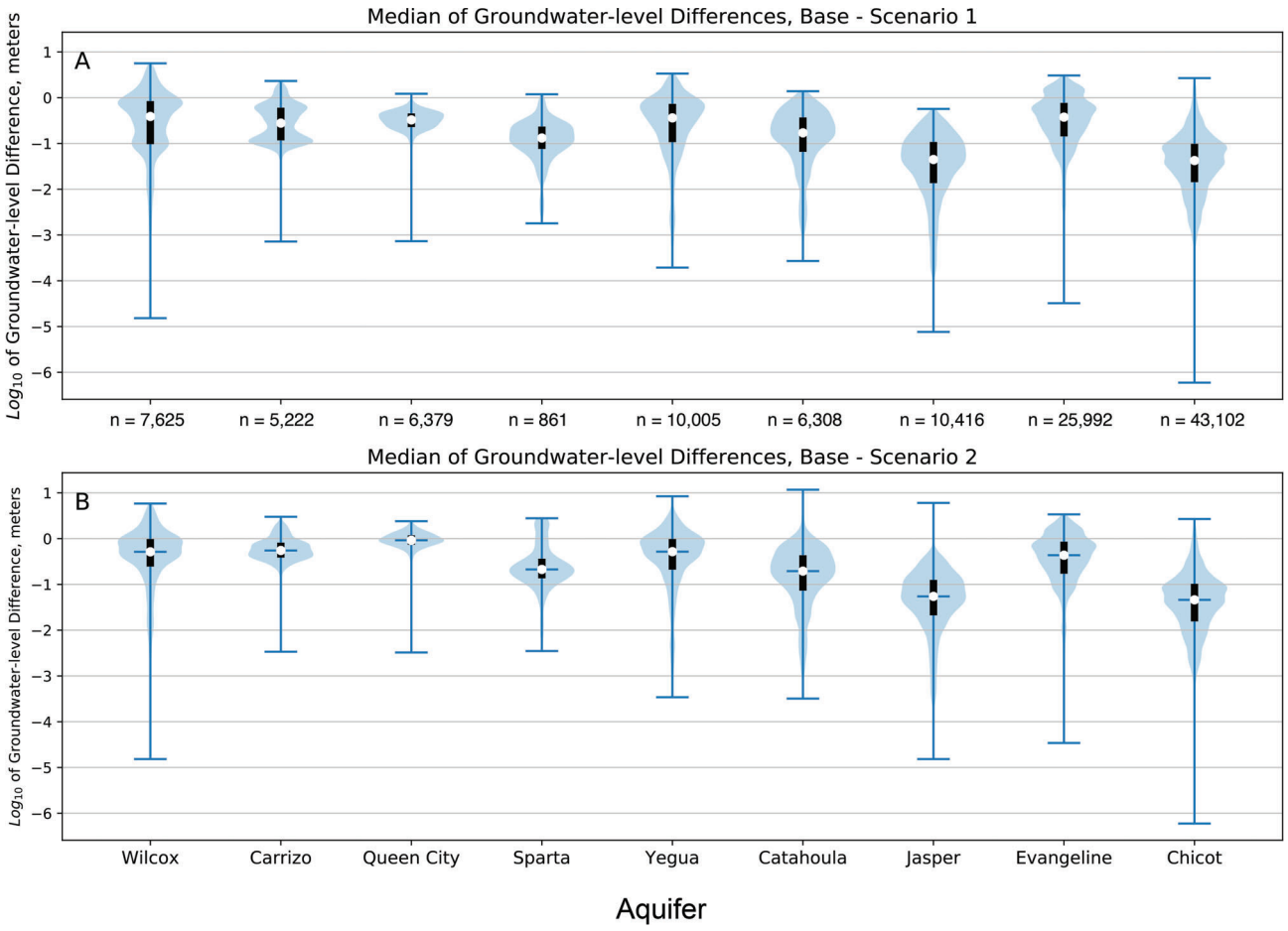

Figure 8. Violin plots showing the median groundwater-level differences per aquifer in layer 1. White dots indicate the median, the black area indicates the 25th to 75th percentile, and the vertical blue bars indicate the extent of the range of values. Number of values (e.g., $n = 5222$) plotted in each violin plot is shown underneath figure A and is the same for both figures.

reducing base flows and groundwater levels for some time (Barlow and Leake 2012). Therefore, the analyses presented herein are useful for short-term planning horizons, no longer than 8 years. Longer transient models would need to be developed for longer-term planning of more than 8 years.

The response of the surface-water/groundwater exchange to a 25% reduction in recharge combined with a 1% and 25% increase in groundwater pumping shows varying degrees of reduction of simulated base flow from the upstream gage near Elmendorf to the farthest downstream gage of interest at Goliad. Larger reductions in simulated base flow occur with greater pumpage and farther downstream in the surface-water system. The small estimated changes in simulated base flow at the Elmendorf gage are likely a result of its location near the upstream end of the basin, where base flow and groundwater are affected by fewer parameters, and therefore less uncertainty, inside its contributing area.

Groundwater levels vary across the study area both in the shallow groundwater system and in the deeper system. In the shallow groundwater system, the water levels are expected to decrease, on average, less than 1 m over an 8-year scenario period, based on the expected value (i.e., the central tendency of the median changes). However, localized water-level declines, such as those near pumping wells, could potentially be much larger. Variability in results across aquifers in the shallow groundwater system is appreciable and some aquifers show similar results for scenario 1 and scenario 2, whereas other aquifers show sensitivity to the increases in groundwater withdrawals between scenario 1 and scenario 2.

The results of this analysis demonstrate that the basin may be susceptible to drought and increases in groundwater withdrawals even on a short planning horizon, such as 8 years. A 25% reduction in recharge, combined with a 25% increase in groundwater withdrawals could cause considerable groundwater level reductions and base-flow reductions downstream in the surface-water system. The results also demonstrate the applicability and usefulness of development of the predictive scenarios within a stochastic framework to aid water-resource managers in their decision making with regards to the potential effects of hydrologic changes on the system.

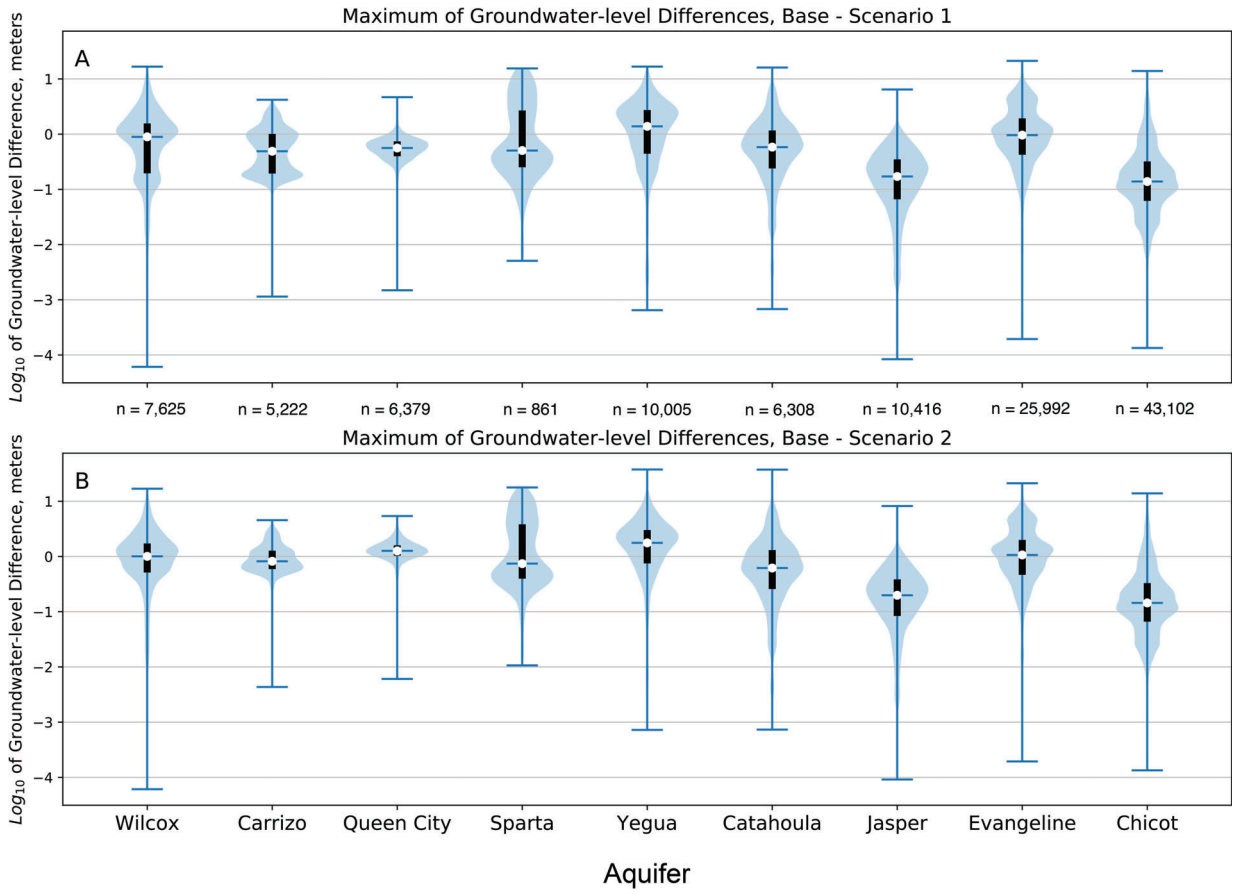

Figure 9. Violin plots showing the maximum groundwater-level differences per aquifer in layer 1. White dots indicate the median, the black area indicates the 25th to 75th percentile, and the vertical blue bars indicate the extent of the range of values. Number of values (e.g., $n = 5222$) plotted in each violin plot is shown underneath figure A and is the same for both figures.

Acknowledgments

We wish to acknowledge the following people for their helpful peer review comments: Martha Nielsen, USGS peer reviewer, Dr. Ty Ferre and two anonymous reviewers. We also thank the Goliad County Groundwater Conservation District, the Evergreen Underground Water Conservation District, and the San Antonio River Authority for providing valuable comments and information. The model files and executables used in the model are available at https://doi.org/10.5066/P9051RUT. This research was funded by the San Antonio River Authority in collaboration with the U.S. Geological Survey. Any use of trade, firm, or product names is for descriptive purposes only and does not imply endorsement by the U.S. Government.

Authors' Note

The authors do not have any conflicts of interest or financial disclosures to report.

Supporting Information

Additional supporting information may be found online in the Supporting Information section at the end of the article. Supporting Information is generally *not* peer reviewed.

Appendix S1. Additional model details such as the active and inactive areas, the array used for implementation of recharge, locations of monitoring wells, locations of pilot points, the *MAP* parameter values and posterior standard deviation, and the *MAP* model water budget. Also included are the modeled versus observed base flow at the main gages, the difference ensembles of the base ensemble and scenario ensembles of base flow at the main gages, and the base ensemble and scenario ensembles of groundwater levels at monitoring wells. However, U.S. Geological Survey information products including supporting information are peer reviewed and approved for publication consistent with Fundamental Science Practices policies (https://pubs.usgs.gov/circ/1367/).

References

Anderson, M.P., W.W. Woessner, and R.J. Hunt. 2015. *Applied Groundwater Modeling: Simulation of Flow and Advective Transport*, 2nd ed., 564. London, UK: Academic Press.

Ashworth, J.B. and J. Hopkins. 1995. Aquifers of Texas, Texas Water Development Board Report 345, 69 p, https://www

.twdb.texas.gov/publications/reports/numbered_reports/doc/r345/r345complete.pdf.
Baker, Jr., E.T. 1979. Stratigraphic and hydrogeologic framework of part of the coastal plain of Texas: Texas Department of Water Resources Report 236, 43 p.
Banta, J.R. and D.J. Ockerman. 2014. Simulation of hydrologic conditions and suspended-sediment loads in the San Antonio River Basin downstream from San Antonio, Texas, 2000-12: U.S. Geological Survey Scientific Investigations Report 2014-5182, 46 p, http://doi.org/10.3133/sir20145182.
Barlow, P.M. and S.A. Leake. 2012. Streamflow depletion by wells—Understanding and managing the effects of groundwater pumping on streamflow, U.S. Geological Survey Circular 1376, 84 p., https://doi.org/10.3133/cir1376.
Barlow, P.M., Cunningham, W.L., Zhai, T., and M. Gray. 2015. U.S. Geological Survey Groundwater Toolbox, a graphical and mapping interface for analysis of hydrologic data (version 1.0): User guide for estimation of base flow, runoff, and groundwater recharge from streamflow data: U.S. Geological Survey Techniques and Methods 3-B10, 27 p., https://doi.org/10.3133/tm3b10.
Bonesky, T. 2008. Morozov's discrepancy principle and tikhonov-type functionals. *Inverse Problems* 25, no. 1. 015015. https://doi.org/10.1088/0266-5611/25/1/015015
Chowdhury, A.H., Wade, S., Mace, R.E., and C. Ridgeway. 2004. Groundwater availability model of the central Gulf Coast aquifer system: Numerical simulations through 1999, Texas Water Development Board, 114 p., https://www.twdb.texas.gov/groundwater/models/gam/glfc_c/twdb_recalibration_report.pdf.
Clark, B.R. and R.M. Hart. 2009. The Mississippi Embayment Regional Aquifer Study (MERAS): Documentation of a groundwater-flow model constructed to assess water availability in the Mississippi Embayment: U.S. Geological Survey Scientific Investigations Report 2009-5172, 61 p.
Deeds, N.E., Yan, T., Singh, A., Jones, T., Kelley, V., Knox, P., and S. Young. 2010. Final report groundwater availability model for the Yegua-Jackson Aquifer, Texas Water Development Board, 582 p., http://www.twdb.texas.gov/groundwater/models/gam/ygjk/ygjk_model_report.pdf.
Doherty, J.E. 2015. *Pest and its Utility Support Software, Theory*, 366. Brisbane, Australia: Watermark Numerical Publishing.
Doherty, J., and C. Moore. 2019. Decision support modeling: Data assimilation, uncertainty quantification, and strategic abstraction. *Groundwater* 58, no. 3: 327–337.
Doherty, J.E., and D. Welter. 2010. A short exploration of structural noise. *Water Resources Research* 46, no. 5. https://doi.org/10.1029/2009wr008377
Doherty, J.E., Fienen, M.N., and M.J. Tonkin. 2010a. Approaches to highly parameterized inversion: Pilot-point theory, guidelines, and research directions, U.S. Geological Survey Scientific Investigations Report 2010-5168, https://doi.org/10.3133/sir20105168.
Doherty, J.E., Hunt, R.J., and M.J. Tonkin. 2010b. Approaches to highly parameterized inversion: A guide to using pest for model-parameter and predictive-uncertainty analysis, U.S. Geological Survey Scientific Investigations Report 2010-5211, 71 p., http://pubs.usgs.gov/sir/2010/5211.
Dutton, A.R. 2004. Pumping metadata associated with conceptualization and simulation of the Edwards aquifer, San Antonio, Texas. Technical report, Bureau of Economic Geology.
Dutton, A.R., Harden, B., Nicot, J.P., O'Rourke, D., Harden, B., O'Rourke, D., and R. Harden. 2003. *Groundwater availability model for the central part of the Carrizo-Wilcox aquifer in Texas*. Prepared for the Texas Water Development Board, Austin, Texas: The University of Texas at Austin, Bureau of Economic Geology, http://www.twdb.texas.gov/groundwater/models/gam/czwx_c/czwx_c_full_report.pdf.
Foster, L.K. 2020. MODFLOW-NWT model for risk-based decision-support groundwater modeling for the lower San Antonio River Basin, Texas, USA, U.S. Geological Survey Data Release, https://doi.org/10.5066/p9051rut.
Ground Water Protection Council and Interstate Oil and Gas Compact Commission (IOGCC). 2017. FracFocus Chemical Disclosure Registry v 2.0. https://fracfocus.org/.
Kelley, V., N. Deeds, D. Fryar, and J. Nicot. 2004. Groundwater availability models for the Queen City and Sparta aquifers: Contract report to the Texas Water Development Board, 867.
Knowling, M.J., J.T. White, and C.R. Moore. 2019. Role of model parameterization in risk-based decision support: An empirical exploration. *Advances in Water Resources* 128: 59–73. https://doi.org/10.1016/j.advwatres.2019.04.010
Lizárraga, J.S. and D.J. Ockerman. 2010. Simulation of streamflow, evapotranspiration, and groundwater recharge in the lower San Antonio River watershed, south-central Texas, 2000-2007: U.S. Geological Survey Scientific Investigations Report 2010-5027, 41 p., https://doi.org/10.3133/sir20105027.
Lizárraga, J.S. and L.L. Wehmeyer. 2012. Estimation of streamflow gains and losses in the lower San Antonio River watershed, south-central Texas, 2006-10: U.S. Geological Survey Scientific Investigations Report 2012-5073, 34 p., https://doi.org/10.3133/sir20125073.
Mace, R., Davidson, S., Angle, E., and W. Mullican. 2006. Aquifers of the Gulf Coast of Texas, Texas Water Development Board, Report 365, 312 p.
Maupin, M.A., Kenny, J.F., Hutson, S.S., Lovelace, J.K., Barber, N.L., and K.S. Linsey. 2014. Estimated use of water in the United States in 2010, U.S. Geological Survey Circular 1405, 56 p., https://doi.org/10.3133/cir1405.
McKay, L., T. Bondelid, T. Dewald, J. Johnston, R. Moore, and A. Rea. 2012. *NHDPlus Version 2: User guide*. U.S. Environmental Protection Agency.
Menke, W. 1989. *Geophysical Data Analysis: Discrete Inverse Theory*, 2nd ed. San Diego, California: Academic Press.
Niswonger, R. and D. Prudic. 2005. Documentation of the Streamflow-Routing (SFR2) Package to include unsaturated flow beneath streams—A modification to SFR1, U.S. Geological Survey Techniques and Methods 6-A13, 50 p., https://doi.org/10.3133/tm6a13.
Niswonger, R., Panday, S., and M. Ibaraki. 2011. MODFLOW-NWT, A Newton formulation for MODFLOW-2005, U.S. Geological Survey Techniques and Methods 6-A37, 44 p., https://doi.org/10.3133/tm6a37.
Oliver, D., A. Reynolds, and N. Liu. 2008. *Inverse Theory for Petroleum Reservoir Characterization and History Matching*. Cambridge: Cambridge University Press.
Railroad Commission of Texas. 2019. Texas Eagle Ford shale drilling permits issued 2008 through November 2019, https://www.rrc.state.tx.us/media/55433/eagle-ford-drilling-permits-nov-2019.pdf.
Reitz, M., W.E. Sanford, G. Senay, and J. Cazenas. 2017. Annual estimates of recharge, quick-flow runoff, and evapotranspiration for the contiguous US using empirical regression equations. *Journal of the American Water Resources Association* 53, no. 4: 961–983. https://doi.org/10.1111/1752-1688.12546
Ryder, P. 1996. Ground Water Atlas of the United States: Oklahoma, Texas, U.S. Geological Survey Hydrologic Atlas 730-E, 32 p. https://doi.org/10.3133/ha730e (accessed December 15, 2020)
South Central Texas Regional Water Planning Group. 2015. 2016 South Central Texas Regional Water Plan—Volume 1: Executive Summary and Regional Water Plan. Technical report.
Texas Water Development Board. 2018a. Groundwater database reports. http://www.twdb.texas.gov/groundwater/data/gwdbrpt.asp.

Texas Water Development Board. 2018b. Historical water use estimates. http://www.twdb.texas.gov/waterplanning/waterusesurvey/estimates/index.asp.

Tikhonov, A.N., and V.Y. Arsenin. 1977. *Solutions of Ill-Posed Problems*. Washington, DC/New York: V.H. Winston & Sons/John Wiley & Sons.

U.S. Geological Survey. 2019. National Water Information System data available on the World Wide Web (UGSS Water Data for the Nation). http://doi.org/10.5066/f7p55kjn (accessed October 20, 2019).

Wahl, K.L., and T.L. Wahl. 1995. Determining the flow of Comal Springs at New Braunfels, Texas. *Proceedings of Texas Water* 95, no. 6: 16–17 https://www.usbr.gov/tsc/techreferences/hydraulics_lab/pubs/pap/pap-0708.pdf (December 15, 2020)

Waterstone, P. 2003. Groundwater availability of the central Gulf Coast Aquifer—Numerical simulations to 2050, Central Gulf Coast, Texas, Contract draft report subbmitted to Texas Water Development Board, Austin, Texas (variously paginated).

White, J.T., J.E. Doherty, and J.D. Hughes. 2014. Quantifying the predictive consequences of model error with linear subspace analysis. *Water Resources Research* 50, no. 2: 1152–1173. http://doi.org/10.1002/2013wr014767

White, J.T., M.N. Fienen, and J.E. Doherty. 2016. A python framework for environmental model uncertainty analysis. *Environmental Modelling and Software* 85: 217–228. http://doi.org/10.1016/j.envsoft.2016.08.017

White, J.T., Hunt, R.J., Fienen, M.N., and J.E. Doherty. 2020. PEST++ version 5: a software suite for parameter estimation, uncertainty analysis, management optimization and sensitivity analysis, U.S. Geological Survey Techniques and Methods 7C26, 52 p., https://doi.org/10.3133/tm7c26.

Winters, K.E. 2013. A historical perspective on precipitation, drought severity, and streamflow in Texas during 1951-56 and 2011, U.S. Geological Survey Scientific Investigations Report 2013-5113. https://doi.org/10.3133/sir20135113 (accessed December 15, 2020).